FEBS Letters 543 (2003) 164–169 FEBS 27251

Crystal structure of DsbDγ reveals the mechanism of redox potential shift and substrate specificity[1]

Jae Hoon Kim[2], Seung Jun Kim[2], Dae Gwin Jeong, Jeong Hee Son, Seong Eon Ryu*

Center for Cellular Switch Protein Structure, Korea Research Institute of Bioscience and Biotechnology, 52 Euh-eun-dong, Yusong-gu, Daejon 305-806, South Korea

Received 26 February 2003; revised 15 April 2003; accepted 15 April 2003

First published online 1 May 2003

Edited by Hans Eklund

Abstract The *Escherichia coli* transmembrane protein DsbD transfers electrons from the cytoplasm to the periplasm through a cascade of thiol-disulfide exchange reactions. In this process, the C-terminal periplasmic domain of DsbD (DsbDγ) shuttles the reducing potential from the membrane domain (DsbDβ) to the N-terminal periplasmic domain (DsbDα). The crystal structure of DsbDγ determined at 1.9 Å resolution reveals that the domain has a thioredoxin fold with an extended N-terminal stretch. In comparison to thioredoxin, the DsbDγ structure exhibits the stabilized active site conformation and the extended active site α2 helix that explain the domain's substrate specificity and the redox potential shift, respectively. The hypothetical model of the DsbDγ:DsbDα complex based on the DsbDγ structure and previous structural studies indicates that the conserved hydrophobic residue in the C-X-X-C motif of DsbDγ may be important in the specific recognition of DsbDα.

Key words: DsbDγ; Crystal structure; Thiol-disulfide exchange reaction; Redox potential; Electron transfer

1. Introduction

In bacteria, disulfide bonds are usually formed in the periplasm where the newly synthesized proteins are rapidly oxidized by the soluble periplasmic protein DsbA [1]. The reduced DsbA transfers electrons to the inner membrane protein DsbB that is coupled with the respiratory chain [2,3]. On the other hand, DsbC and DsbG are known to have the protein disulfide isomerase activity that reduces incorrectly formed disulfide bonds and facilitates correct folding of proteins in the periplasm [4–7]. DsbC and DsbG receive the reducing power from the cytoplasm since the periplasmic space is an oxidizing environment. The inner membrane protein DsbD transfers electrons from the cytoplasmic thioredoxin to the periplasmic DsbC and DsbG across the membrane [8–11].

DsbD consists of three domains: α, β and γ domains [12]. DsbDα and DsbDγ are located in the periplasmic space, whereas DsbDβ is a transmembrane domain comprising eight transmembrane helices. Each domain of DsbD has a pair of reactive cysteines and a cascade of inter-domain thiol-disulfide exchange reactions between the sets of reactive cysteines mediates the across-membrane electron transfer [10,11]. The electron transfer function of DsbD can be reconstituted by mixing independently expressed domains, indicating that the three domains of DsbD are separable functional units [13]. Extensive biochemical and mutagenesis studies found that the sequence of electron transfer among the domains is DsbDβ→DsbDγ→DsbDα, thus indicating that DsbDγ is the electron carrier between the other two domains [10,11,14]. DsbDγ specifically recognizes DsbDα for the electron transfer and does not interact with periplasmic disulfide isomerases, DsbC and DsbG [13]. There was a nuclear magnetic resonance peak assignment note for DsbDγ [15]. However, the structure has not been reported yet. To understand the electron shuttling mechanism and the substrate recognition of DsbDγ, we determined the crystal structure of DsbDγ. The structure reveals the domain's unique structural features that enable its function as a specific electron shuttle during the transport of the cytoplasmic reduction potential to the periplasm. In addition, the structural information should be an important guide in future studies to shed light on the whole machinery of DsbD for the electron transfer across the inner membrane.

2. Materials and methods

DsbDγ (residues 423–546) was expressed in *Escherichia coli* BL21(DE3) and B834(DE3) cells for the native and the selenomethionine-labeled proteins, respectively. The *E. coli* cells were harvested and lysed by sonication in a lysis buffer containing 50 mM Tris–HCl (pH 7.5), 150 mM NaCl and 1.0 mM phenylmethylsulfonyl fluoride. The pellet obtained by ammonium sulfate fractionation (30–60%) was redissolved in a buffer containing 1.5 M ammonium sulfate and 50 mM potassium phosphate (pH 6.8), and the protein was purified using phenyl Sepharose 6 FF, Q-Sepharose and Hiprep 26/60 Sephacryl S200HR column chromatographies. The purified protein was dialyzed against a buffer containing 10 mM HEPES–NaOH (pH 7.0) for use in crystallization.

DsbDγ was crystallized by the hanging drop vapor diffusion method. The best crystals were grown at 25°C by mixing 1.8 μl of protein solution (50 mg/ml) and an equal volume of reservoir solution containing 28% (w/v) PEG 8000, 0.1 M sodium acetate and 0.2 M ammonium acetate (pH 4.6). In the same crystallization condition, two different crystal forms (I and II) were obtained. Both crystal forms belonged to an orthorhombic space group, $P2_12_12_1$. However, their cell constants are completely different (Table 1), and the asymmetric units of form I and II crystals contain one and two molecules of DsbDγ, respectively.

Diffraction data for the structure determination were collected in the beamline 6B at Pohang Accelerator Laboratory with a DIP2030

*Corresponding author. Fax: (82)-42-860 4598.
E-mail address: ryuse@kribb.re.kr (S.E. Ryu).

[1] The atomic coordinates of DsbDγ have been deposited in the Protein Data Bank (ID: 1UC7).
[2] These authors contributed equally to this work.

0014-5793/03/$22.00 © 2003 Published by Elsevier Science B.V. on behalf of the Federation of European Biochemical Societies.
doi:10.1016/S0014-5793(03)00434-4

image plate detector. A form I crystal grown from the SeMet-derivatized DsbDγ was used for the MAD data collection [16]. Prior to the data collection, the crystal was transferred to the reservoir solution supplemented with 10% PEG 400 as a cryo-protectant. The Bijvoet data of 2.3 Å resolution at the peak (λ1), edge (λ2), and remote (λ3) wavelengths were collected at −170°C. A native data set with higher resolution (1.9 Å) was collected from a form II crystal at room temperature using a Rigaku RU300 generator with an R-AXIS IV^{++} image plate detector (Table 1). The MAD data and native data sets were processed with the HKL program suite [17] and the program MOSFLM [18], respectively. The CCP4 program suite [18] also was used for further data processing and analysis. Two selenium positions were located and refined with the program SOLVE [19]. The phases were calculated to 2.3 Å using the program SHARP [20] and the resulting phases were subjected to density modification with the program SOLOMON [21].

In the initial structure refinement for the form I crystal, the data collected at the peak wavelength (λ1), which had higher data coverage than other wavelengths, were used. The structure obtained from the form I crystal was used as the start structure for the molecular replacement search and further refinement with the higher resolution data collected from the form II crystal (Table 1). The programs O [22] and CNS [23] were used in the model building and refinement, respectively. In the final model (the form II crystal), all residues have good stereochemical geometry as defined by the program PROCHECK [24], where 93.0% of all residues are in the most favored regions and there is none in the disallowed regions. Lys 503, Leu 514, Asp 533, Ser 538, and Arg 544 of one DsbDγ molecule exhibited

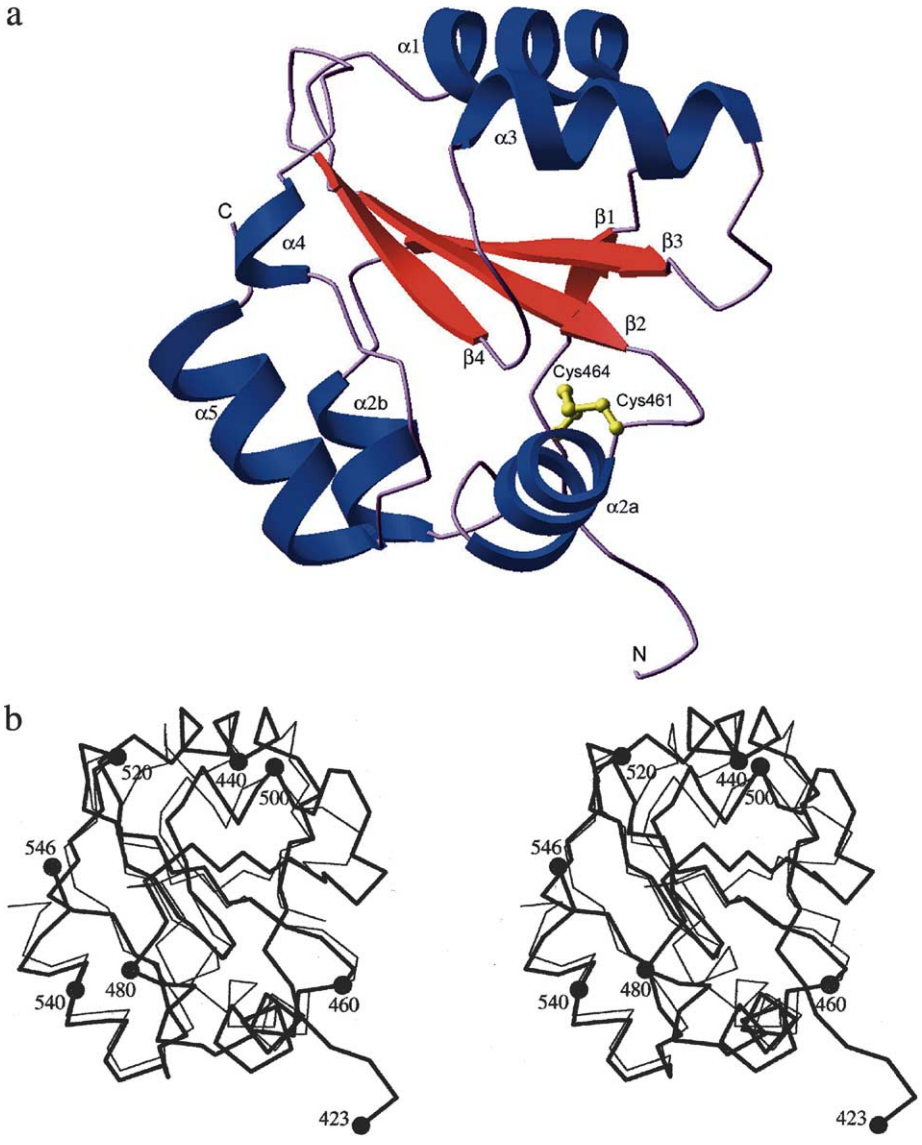

Fig. 1. Overall structure of DsbDγ. a: A schematic ribbon diagram of the monomeric DsbDγ. Secondary structural elements are labeled on the drawing. The active site cysteines participating in a disulfide bond are drawn as a ball-and-stick representation. Boundaries of the secondary structural elements are β1 (431–432), β2 (452–457), β3 (485–490), β4 (512–516), α1 (437–446), α2a (462–470), α2b (475–480), α3 (496–505), α4 (524–526) and α5 (534–544). b: Structural comparison of DsbDγ (thick line) with *E. coli* thioredoxin (thin line). Cα traces of the two structures are superimposed using the program O [22]. The point of view is the same as in panel a. Cα positions of every twentieth residues in the DsbDγ structure are indicated as gray balls and labeled in the stereodiagram. c: Sequence alignment. Sequences of DsbDγ from four different species (*E. coli*, *Yersinia pestis*, *Vibrio cholerae* and *Haemophilus influenza*) and that of the *E. coli* thioredoxin are aligned together using the program CLUSTALW [32]. Secondary structural elements of the *E. coli* DsbDγ are shown above aligned sequences, whereas those of the *E. coli* thioredoxin are below the sequences. The residues with 100% identity are colored orange and those with conservation values above 5.0 defined in the program ALSCRIPT [33] are colored yellow. The active site cysteines are indicated with inverted triangles.

alternative side chain densities and the alternative conformations were included in the refinement. The final model includes residues 423–546 of both DsbDγ molecules in the asymmetric unit and 117 water molecules.

3. Results and discussion

DsbDγ (423–546) folds into a compact and globular domain of approximate dimensions 35 Å×30 Å×25 Å. Two DsbDγ monomers in the asymmetric unit have essentially the same conformation. Each DsbDγ molecule contains six α-helices (α1, α2a, α2b and α3–α5) and four β-strands (β1–β4), resulting in a thioredoxin fold (Fig. 1). Despite the modest sequence identity (24%) between DsbDγ and *E. coli* thioredoxin, the two structures are well aligned and the Cα atom superposition yields a root mean square deviation of 1.54 Å for 91 out of 105 residues (Fig. 1b). The C-X-X-C motif of DsbDγ (Cys 461-Val 462-Ala 463-Cys 464) is located at the N-terminus of helix α2a. The disulfide bridge between the two active site cysteines is evident in the electron density map (Fig. 2), consistent with the non-reducing condition in the crystallization setup. The disulfide bond has a similar conformation to that of the oxidized *E. coli* thioredoxin [25].

There are several important structural differences between DsbDγ and thioredoxin. The region of DsbDγ corresponding to the kink helix α2 of thioredoxin exhibits a longer helix with more pronounced helix kink with the four-residue insertion, resulting in two separated helices (α2a, α2b). The stabilization of the active site cysteine thiolate in the thioredoxin fold oxidoreductases is necessary for the reactivity of the cysteine, and the helix dipole of helix α2 is thought to play an important role in the thiolate stabilization of the thioredoxin family proteins [26]. The helix kink in the thioredoxin α2 helix distorts the hydrogen bond array and limits the length of the helix with intact hydrogen bond array to eight residues (Cys 32 to Ala 39) [25]. In comparison, the DsbDγ α2a helix comprises 13 residues (Cys 461 to Ser 473) that form a continuous helical hydrogen bond array, strengthening the helix dipole (Fig. 1). Recently, Collet et al. [13] determined the redox potential of DsbDγ to be −241 mV, which was substantially different from that of *E. coli* thioredoxin (−270 mV). Since the magnitude of the helix dipole is correlated with the length of the helix [27], the longer active site helix α2a in DsbDγ should stabilize the active site cysteine thiolate more and shift the redox potential towards the oxidizing direction.

In comparison to the thioredoxin active site flexibility that was implicated in the substrate recognition [28,29], the active site region of DsbDγ appears to have tighter interaction networks than that of thioredoxin. In thioredoxin, residues in the β3-α2 loop immediately preceding the C-X-X-C motif does not form strong interactions with neighboring residues. The corresponding region of DsbDγ forms extensive hydrogen bond interactions with neighbors (Fig. 2). In addition, the gap surrounded by β2, β3 and α2 near the active site of thioredoxin is filled with the side chain of Tyr 457 in DsbDγ, strengthening the stability of the region. These stabilizing interactions in the active site of DsbDγ are likely to contribute to the DsbDγ strict substrate specificity to DsbDα. However, the correlation between the stabilized active site and the substrate specificity is a speculative postulation and should be tested by future biochemical studies.

The four N-terminal residues (423–426) of DsbDγ are stretched away from the main body of the molecule (Fig. 1a,b). Since the last transmembrane helix of DsbDβ ends at His 421 [11], the residues 422–426 region is likely to play as a linker between the core regions of DsbDβ and DsbDγ. In the crystal of DsbDγ, the N-terminal stretch (residues 423–426) of one molecule in the asymmetric unit forms antiparallel β-bridge interactions with the same N-terminal residues of the other molecule, which stabilizes the projecting strands. The β-bridge interactions result in a non-crystallographic two-fold related dimer of DsbDγ. However, other regions of

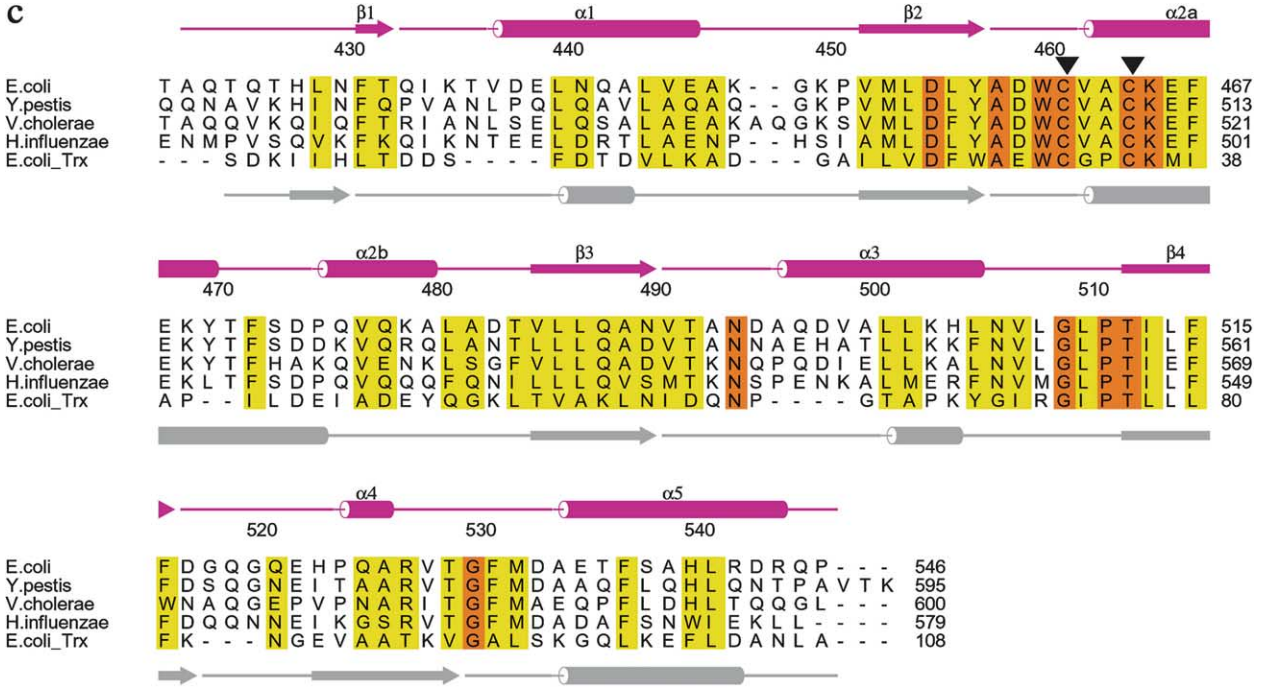

Fig. 1 (*Continued*).

Table 1
Crystallographic data and refinement statistics

	SeMet			Native
A. Data collection and phasing statistics				
	Peak (λ1)	Edge (λ2)	Remote (λ3)	
Wavelength (Å)	0.9795	0.9792	0.9717	1.5418
Space group	$P2_12_12_1$			$P2_12_12_1$
Cell dimension (Å)	30.27×44.57×73.18			30.33×57.66×126.60
Highest resolution (Å)	2.3	2.5	2.5	1.9
Unique reflections (total)	4559 (57 953)	3516 (37 529)	3518 (37 567)	17 648 (60 479)
Completeness (%)[a]	95.7 (93.1)	94.6 (97.2)	94.6 (96.7)	96.8 (84.3)
R_{merge} (%)[b]	5.9 (15.2)	6.8 (14.3)	5.5 (13.1)	9.1 (19.4)
$I/\sigma(I)$	28.3 (8.0)	21.1 (9.3)	20.5 (8.4)	4.5 (3.0)
Phasing power				
Acentric/centric[c]	–/–	2.4/1.5	2.1/1.3	
Anomalous	2.3	3.1	2.7	
B. Refinement statistics				
Resolution range (Å)	99–2.3			99–1.9
Number of reflections	4487			17 604
Number of atoms (protein/non-protein)	941/21			1951/118
R_{cryst} [d]	23.2			18.5
R_{free} [e]	28.1			21.8
Rms deviations				
Bond lengths (Å)	0.006			0.005
Bond angles (°)	1.19			1.15
Impropers (°)	0.74			0.67
Dihedrals (°)	24.04			23.2

[a]The values in parentheses (completeness and R_{merge}) are for the highest resolution bin.
[b]$R_{merge} = \Sigma_i |I_i - \langle I \rangle| / \Sigma |\langle I \rangle|$, where I is the intensity for the ith measurement of an equivalent reflection with the indices h,k,l.
[c]Phasing power = F_H/E, where F_H is the heavy-atom structure factor amplitude and E is the lack-of-closure error.
[d]$R_{cryst} = \Sigma |F_o - F_c| / \Sigma F_o$, where F_o and F_c are the observed and calculated structure factor amplitudes, respectively.
[e]The R_{free} value was calculated from 5% of all data that were not used in the refinement.

the protein do not make significant dimeric interactions and our preliminary analyses on the oligomeric state of DsbDγ by gel filtration chromatography and dynamic light scattering indicate that DsbDγ exists as a monomer in solution (data not shown). Thus, it is likely that the non-crystallographic dimer has no physiological significance. Since DsbDγ has to shuttle electrons between DsbDβ and DsbDα, one could hypothesize that there might be a physical movement of DsbDγ during the electron shuttling. In that case, the flexible N-terminal stretch of DsbDγ may be a joint for the domain motion during the DsbDγ electron shuttling between DsbDβ and DsbDα. In the DsbDγ structure, there is a cleft formed by the kink region between helices α2a and α2b, and the central β-sheet. Residues following the flexible N-terminal region of DsbDγ go through the cleft and make strong interactions with the cleft. For example, Leu 429 immediately following the flexible N-terminus makes hydrophobic interactions with side chains of Phe 472, Leu 481, and Leu 486 in the middle of the cleft. The side chain of Phe 431 also makes strong interactions with Phe 472, Leu 486 and Met 453 in the cleft region. These unique interactions are likely to play an important role in stabilizing the fold of DsbDγ during the domain motion utilizing the flexible N-terminal region. The residues involved in the interactions would be good targets for mutagenesis studies to understand the electron shuttling mechanism of DsbDγ between the β and α domains.

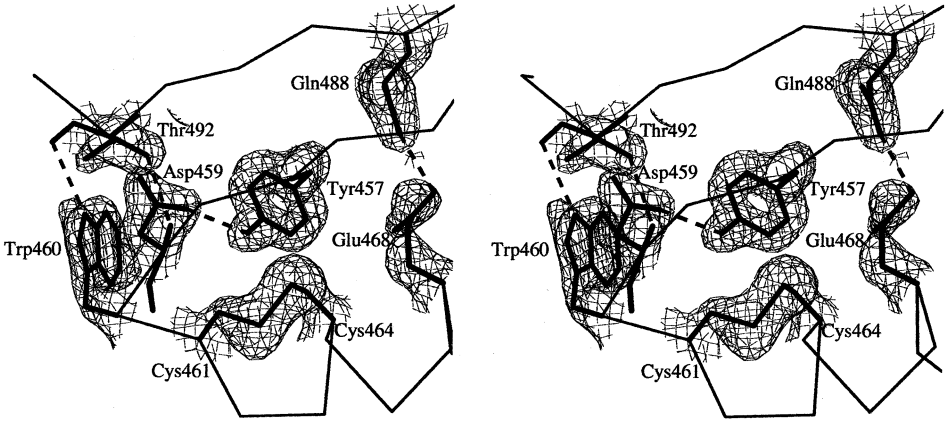

Fig. 2. Active site stability. Side chains of the residues participating in hydrogen bonds near the active site cysteines are presented as thick lines on the Cα trace drawing (thin line) in the stereodiagram. Potential hydrogen bond interactions (inter-atomic distances < 3.2 Å) are indicated as broken lines. Interactions shown in the figure are Thr 492 (O):Trp 460 (NE1) (3.1 Å); Thr 492 (OG1):Asp 459 (N) (2.87 Å); Asp 459(OD1):Tyr 457 (OH) (2.58 Å) and Glu 468 (OE1):Gln 488 (NE2) (2.80 Å). The $2F_o - F_c$ electron density map was calculated for the regions including 2.0 Å spheres surrounding the side chain atom positions. The map is contoured at 1.0σ level.

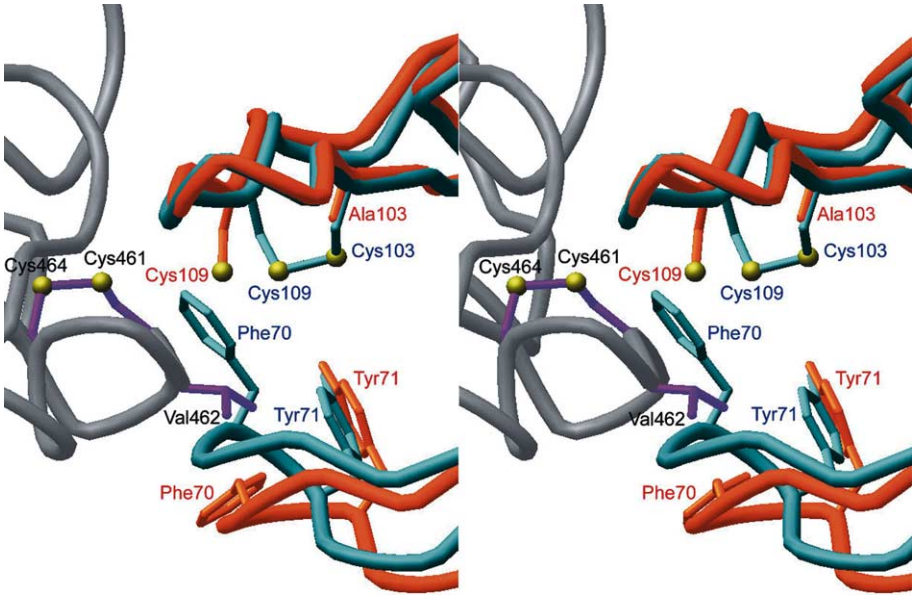

Fig. 3. A hypothetical model for the interaction between DsbDγ and DsbDα. The model for DsbDγ-DsbDα interaction was created by superposing the DsbDγ structure on the DsbC region of the DsbC-DsbDα complex structure (PDB ID: 1JZD). In the figure, the hypothetical DsbDγ-DsbDα interface around the active site cap region is presented. Side chains of the representative residues in the interface are drawn as sticks on the Cα trace diagrams of the DsbDγ (main chain: gray; side chain: violet), the open form DsbDα (main and side chains: orange) and the closed form DsbDα (main and side chains: cyan) structures. The sulfur atoms in the active site cysteine residues are indicated as yellow balls. In the open form DsbDα structure, Cys 103 was mutated to Ala 103 for crystallization [30]. The closed form DsbDα structure (PDB ID:1JPE) was drawn as superposed with the open form structure in the DsbC-DsbDα complex structure.

Recently, the structure of the DsbC-DsbDα complex revealed the interaction and recognition mechanism between DsbC and DsbDα [30]. In the complex structure, the dimeric DsbC binds to the DsbDα monomer utilizing two independent DsbC binding sites and the primary binding interactions occur between the catalytic C-X-X-C motif region of DsbC and the active site cap region of DsbDα. Since DsbC has a thioredoxin fold like DsbDγ, we used the DsbC-DsbDα complex structure to gain insight into the possible interactions between DsbDγ and DsbDα by superimposing the DsbDγ structure on the DsbC region of the DsbC-DsbDα complex structure (Fig. 3). The Cα carbon superposition between DsbDγ and DsbC yields a root mean square deviation of 1.67 Å for 65 Cα carbon atoms. Although there is no convincing evidence for the speculative assumption that DsbDγ may interact with DsbDα in the same mode as the DsbC-DsbDα complex, our model based on the assumption indicates interesting possibilities for the mechanism of specific interaction between DsbDγ and DsbDα. In the model, the superposed DsbDγ forms a complementary interface with the DsbDα molecule in the complex and there are no noticeable clashes between residues of DsbDγ and DsbDα, indicating that DsbDγ can bind DsbDα without major conformational rearrangement. In the DsbC-DsbDα complex structure, the highly conserved aromatic side chain of Tyr 100 of DsbC, which binds into the pocket near the DsbDα active site, plays an important role in lifting the active site cap of DsbDα [30]. The corresponding residue in DsbDγ is Ala 463, which does not have a bulky side chain. However, the adjacent residue, Val 462 of DsbDγ, appears to play an important role in the cap opening. The hydrophobic side chain of the DsbDγ Val 462 clashes into the cap residue Phe 70 of the closed form DsbDα [30,31], whereas the same residue fits well with the cavity that results from the conformation change in the loop containing Phe 70 in the open form DsbDα [29] (Fig. 3). Thus, the DsbDγ Val 462 is likely to play a critical role in the cap opening in the active site of DsbDα and the specific electron transfer between DsbDγ and DsbDα. It is noteworthy that Val 462 and Ala 463 are the dipeptide residues in the C-X-X-C motif. Val 462 is highly conserved in DsbDγ of various organisms (Fig. 1c), supporting the residue's important role in the function of DsbDγ. Future biochemical studies involving mutations of Val 462 are likely to provide insight into the mechanism of specific interaction between DsbDγ and DsbDα.

Acknowledgements: We thank Dr. H.-S. Lee at the Pohang Accelerator Laboratory for help in data collection. We also thank Dr. P. Metcalf for providing the coordinates of the DsbC:DsbDα complex structure before public release.

References

[1] Bardwell, J.C., McGovern, K. and Beckwith, J. (1991) Cell 67, 581–589.
[2] Guilhot, C., Jander, G., Martin, N.L. and Beckwith, J. (1995) Proc. Natl. Acad. Sci. USA 92, 9895–9899.
[3] Bader, M., Muse, W., Ballow, D.P., Gassner, C. and Bardwell, J.C. (1999) Cell 98, 217–227.
[4] Shevchik, V.E., Condemine, G. and Robert-Baudouy, J. (1994) EMBO J. 13, 2007–2012.
[5] Missiakas, D., Georgopoulos, C. and Raina, S. (1994) EMBO J. 13, 2013–2020.
[6] Zapun, A., Missiakas, D., Raina, S. and Creighton, T.E. (1995) Biochemistry 34, 5075–5089.
[7] Bessette, P.H., Cotto, J.J., Gilbert, H.F. and Georgiou, G. (1999) J. Biol. Chem. 274, 7784–7792.
[8] Krupp, R., Chan, C. and Missiakas, D. (2001) J. Biol. Chem. 276, 3696–3701.
[9] Bader, M.W., Hiniker, A., Regeimbal, J., Goldstone, D., Haebel, P.W., Riemer, J., Metcalf, P. and Bardwell, J.C. (2001) EMBO J. 20, 1555–1562.

[10] Katzen, F. and Beckwith, J. (2000) Cell 103, 769–779.
[11] Chung, J., Chen, T. and Missiaka, D. (2000) Mol. Microbiol. 35, 1099–1109.
[12] Missiakas, D., Schwager, F. and Raina, S. (1995) EMBO J. 14, 3415–3424.
[13] Collet, J.F., Riemer, J., Bader, M.W. and Bardwell, J.C. (2002) J. Biol. Chem. 277, 26886–26892.
[14] Katzen, F., Deshmukh, M., Daldal, F. and Beckwith, J. (2002) EMBO J. 21, 3960–3969.
[15] Bushell, K.M.W., Ferguson, S.J. and Redfield, C. (2002) J. Biomol. NMR 24, 359–360.
[16] Hendrickson, W.A. and Ogata, C.M. (1997) Methods Enzymol. 276, 494–523.
[17] Otwinowski, Z. and Minor, W. (1997) Methods Enzymol. 276, 307–326.
[18] Collaborative Computational Project Number 4 (1994) Acta Crystallogr. D50, 760–763.
[19] Terwilliger, T.C. and Berendzen, J. (1999) Acta Crystallogr. D55, 849–861.
[20] de La Fortelle, E. and Bricogne, G. (1997) Methods Enzymol. 276, 472–494.
[21] Abrahams, J.P. and Leslie, A.G. (1996) Acta Crystallogr. D52, 30–42.
[22] Jones, T.A., Zou, J.Y., Cowan, S.W. and Kjeldgaard, M. (1991) Acta Crystallogr. A47, 110–119.
[23] Brunger, A.T., Adams, P.D., Clore, G.M., DeLano, W.L., Gros, P., Grosse-Kunstleve, R.W., Jiang, J.S., Kuszewski, J., Nilges, M., Pannu, N.S., Read, R.J., Rice, L.M., Simonson, T. and Warren, G.L. (1998) Acta Crystallogr. D54, 905–921.
[24] Laskowski, R.A., MacArthur, M.W., Moss, D.S. and Thornton, J.M. (1993) J. Appl. Crystallogr. 26, 283–291.
[25] Katti, S.K., LeMaster, D.M. and Eklund, H. (1990) J. Mol. Biol. 212, 167–184.
[26] Kortemme, T. and Creighton, T.E. (1995) J. Mol. Biol. 253, 799–812.
[27] Wada, A. (1976) Adv. Biophys. 9, 1–63.
[28] Jeng, M.F., Campbell, A.P., Begley, T., Holmgren, A., Case, D.A., Wright, P.E. and Dyson, H.J. (1994) Structure 2, 853–868.
[29] Capitani, G., Markovic-Housley, Z., DelVal, G., Morris, M., Jansonius, J.N. and Schurmann, P. (2000) J. Mol. Biol. 302, 135–154.
[30] Haebel, P.W., Goldstone, D., Katzen, F., Beckwith, J. and Metcalf, P. (2002) EMBO J. 21, 4774–4784.
[31] Goulding, C.W., Saqaya, M.R., Parseghian, A., Lim, V., Eisenberg, D. and Missiaka, D. (2002) Biochemistry 41, 6920–6927.
[32] Thompson, J.D., Higgins, D.G. and Gibson, T.J. (1994) Nucleic Acids Res. 22, 4673–4680.
[33] Barton, G.J. (1993) Protein Eng. 6, 37–40.